Quantifying Diurnal Cloud Radiative Effects by Cloud Type in the Tropical Western Pacific

CASEY D. BURLEYSON, CHARLES N. LONG,* AND JENNIFER M. COMSTOCK

Pacific Northwest National Laboratory, Richland, Washington

(Manuscript received 29 October 2014, in final form 3 March 2015)

ABSTRACT

Cloud radiative effects are examined using long-term datasets collected at the U.S. Department of Energy's three Atmospheric Radiation Measurement Program Climate Research Facilities in the tropical western Pacific Ocean. The surface radiation budget, cloud populations, and cloud radiative effects are quantified by partitioning the data by cloud type, time of day, and large-scale modes of variability such as El Niño–Southern Oscillation (ENSO) phase and wet/dry seasons at Darwin, Australia. The novel aspect of this analysis is the breakdown of aggregate cloud radiative effects by cloud type across the diurnal cycle. The Nauru Island (Republic of Nauru) cloud populations and subsequently the surface radiation budget are strongly impacted by ENSO variability, whereas the cloud populations over Manus Island (Papua New Guinea) shift only slightly in response to changes in ENSO phase. The Darwin site exhibits large seasonal monsoon-related variations. When present, deeper convective clouds have a strong influence on the amount of radiation that reaches the surface. Their limited frequency reduces their aggregate radiative impact, however. The largest source of shortwave cloud radiative effects at all three sites comes from low clouds. The observations are used to demonstrate that potential model biases in the amplitude of the diurnal cycle and mean cloud frequency would lead to larger errors in the surface energy budget when compared with biases in the timing of the diurnal cycle of cloud frequency. These results provide solid benchmarks to evaluate model simulations of cloud radiative effects in the tropics.

1. Introduction

On average, clouds of various types cover roughly two-thirds of Earth's surface, and cloud radiative effects (CRE) play a significant role in moderating Earth's energy balance (e.g., Arking 1991; Mace et al. 2009; Stubenrauch et al. 2013). Reflection, scattering, and absorption of solar radiation by clouds reduces the global mean top-of-atmosphere (TOA) shortwave (SW) radiative flux by $-46.6\,\mathrm{W\,m^{-2}}$ and enhances the mean longwave (LW) radiative flux by $+29.5\,\mathrm{W\,m^{-2}}$, leading to an average total (SW + LW) TOA CRE of $-17.1\,\mathrm{W\,m^{-2}}$ (Loeb et al. 2009). There is large spatial and temporal variability in the magnitude of CRE across the globe (Kuang et al. 1998; Cess et al. 2001; Wielicki et al. 2002). This variability is pronounced in the tropics, where the mean surface SW CRE can exceed $-95\,\mathrm{W\,m^{-2}}$, or 30% of the mean clear-sky SW radiative flux at the surface (McFarlane et al. 2013; their Table 2). Net radiative cooling from tropical clouds can impact the general circulation of the atmosphere by modifying the equatorial energy budget (Slingo and Slingo 1988; Randall et al. 1989; Chen et al. 2002). Therefore, correctly capturing the radiative impact of clouds in the tropics is critical to correctly simulating tropical forcing in general circulation models (GCMs).

Failure to adequately simulate the frequency and radiative properties of clouds leads to large uncertainties in projections of future climate (Colman 2003; Soden and Held 2006; Webb et al. 2006; Dufresne and Bony 2008). Despite their recognized importance and considerable effort on the part of the GCM community, many cloud types remain poorly simulated in modern GCMs (Li et al. 2012; Su et al. 2013; Klein et al. 2013). Coarse-resolution models often have large biases in the total frequency of

* Current affiliation: Cooperative Institute for Research in Environmental Sciences, NOAA/Earth Systems Research Laboratory, Boulder, Colorado.

Corresponding author address: Dr. Casey D. Burleyson, Pacific Northwest National Laboratory, P.O. Box 999/MS K9-24, Richland, WA 99352.
E-mail: casey.burleyson@pnnl.gov

DOI: 10.1175/JAMC-D-14-0288.1

cloud occurrence as well as the relative frequencies of different cloud types [see, e.g., Klein et al. (2013) and references therein]. There are also common biases that are related to the timing and amplitude of the diurnal cycle of cloudiness in both GCMs and cloud-resolving models (e.g., Arakawa and Kitoh 2005; Dai 2006; Wang et al. 2007; Sato et al. 2009). These errors, combined with an inconsistent treatment of clouds across various model types and resolutions, contribute to large intramodel spreads in the radiative impact of clouds and uncertainty in parameters such as the cloud feedback on the global energy budget (Dufresne and Bony 2008).

At least part of the problem in evaluating and constraining CRE is the underutilization of long-term datasets that measure both cloud properties and the surface radiation budget in climate-sensitive areas. Previous studies have often relied on satellite-based TOA energy budgets to examine CRE in the tropics (e.g., Chen et al. 2000; Loeb et al. 2009). By focusing only on TOA effects, these studies overlook the critical role that tropical clouds play in modifying the surface energy budget (Stephens 2005). Several studies have documented the relationship between clouds and the surface energy budget but have been limited in time or location (e.g., McFarlane et al. 2005; Mace et al. 2006; Wang et al. 2011) or have focused only on a specific cloud type (Jensen and Del Genio 2003; Comstock et al. 2013).

The long-term measurements in the tropical western Pacific Ocean (TWP) carried out by the U.S. Department of Energy (DOE) Atmospheric Radiation Measurement Program (ARM) allow for a detailed examination of surface CRE by cloud type (Mather et al. 1998; Long et al. 2013). ARM has collected observations of clouds and surface radiation at three sites—Manus Island (Papua New Guinea), Nauru Island (Republic of Nauru), and Darwin (Australia)—in the TWP (Long et al. 2013; their Fig. 1). McFarlane et al. (2013) used these datasets to characterize and quantify surface CRE in the tropics. Our study builds upon and expands their work. Two notable differences are the extension of the dataset to include more recent measurements at all three sites and partitioning of the data to examine the diurnal cycle of cloud frequency and CRE. We utilize datasets from all three sites to address the following three questions:

1) What are the primary sources of variability in CRE for tropical clouds?
2) What types of tropical clouds have the largest impact on the surface energy budget?
3) How much would model biases in tropical cloud frequency or the timing of cloud occurrence across the diurnal cycle modify the aggregate CRE?

Our goal is to establish a more robust picture of the sources and magnitude of CRE variability and to establish benchmarks that can be used to evaluate CRE in numerical simulations.

2. Data

a. Cloud profiles and cloud-type classification

The input data and processing steps used in this paper are based on McFarlane et al. (2013). We use ARM data from January 2002 to December 2013 at Manus, from January 2002 to February 2009 at Nauru, and from January 2006 to December 2013 at Darwin. There are intermittent and sometimes sizeable data gaps because of instrument failure. A portion of the time series of data availability is given in McFarlane et al. (2013; their Fig. 2). The underlying surface-radiation and cloud-detection datasets have a base temporal resolution of 1 and 2 min, respectively. We group the 2-min data into 1-h local standard time (LT) increments using the longitude of each site and the UTC time at which the measurement was made. For example, at Manus (2.06°S, 147.43°W) the LT is equal to UTC + 9.83 h; therefore, a measurement made at 1230 UTC would be binned in the 2200–2300 LT window. Data were further subdivided across the diurnal cycle and by El Niño–Southern Oscillation (ENSO) phase for the two equatorial sites and by monsoon seasons for the Darwin site. The number of days of data for each time period and site as well as the mean number of 2-min samples that were averaged together for each 1-h interval across the diurnal cycle is given in Table 1. The large sample that results from the extended data-collection strategies of ARM gives us robust sample sizes, even on hourly time scales.

Cloud properties are measured by several vertically pointing active remote sensing instruments at each site: the millimeter-wavelength cloud radar (MMCR), K_a-band zenith radar (KAZR), laser ceilometer, and micropulse lidar (MPL). The MPL is the primary tool for detecting optically thin high cirrus clouds that exist below the sensitivity threshold of the MMCR and KAZR. The MPL and ceilometer also give more accurate cloud-base heights during periods of precipitation. The two radars provide measurements that are less sensitive to attenuation in deeper clouds. The hydrometeors detected by the active sensors are combined in the Active Remote Sensing of Cloud Layers (ARSCL; Clothiaux et al. 2001) ARM product. Each dataset is averaged onto a common grid with a spatial resolution of 30 m in the vertical direction and a 2-min temporal resolution. Hydrometeors, both cloud and precipitation particles, are identified at each grid point by comparing

TABLE 1. Number of days that each environmental condition was observed at all three sites and the mean number of 2-min samples that were averaged together for each 1-h interval across the diurnal cycle.

		No. of days	Mean No. of 2-min samples available for each 1-h interval
Manus	All data	2097	60 599
	El Niño periods	526	14 474
	Neutral periods	1004	29 510
	La Niña periods	567	16 615
Nauru	All data	806	24 195
	El Niño periods	97	2896
	Neutral periods	299	8982
	La Niña periods	410	12 317
Darwin	All data	1233	36 065
	Dry seasons	411	11 947
	Wet seasons	822	24 118

TABLE 2. Cloud-type definitions as based on the boundaries of each cloud. Definitions are the same as in McFarlane et al. (2013; their Table 3).

Cloud type	Cloud-base height	Cloud-top height	Cloud thickness
Low	<4 km	<4 km	<4 km
Congestus	<4 km	4–8 km	≥1.5 km
Deep convection	<4 km	>8 km	≥1.5 km
Altocumulus	4–8 km	4–8 km	<1.5 km
Altostratus	4–8 km	4–8 km	≥1.5 km
Cirrostratus/anvil	4–8 km	>8 km	≥1.5 km
Cirrus	>8 km	>8 km	No restriction

the radar reflectivity values with absolute thresholds and by looking for vertical gradients in the lidar backscatter (Wang and Sassen 2001). We look for contiguous hydrometeor layers deeper than 120 m (four vertical grid points) in the combined hydrometeor mask and label these as cloud layers. Layers that are spaced less than 120 m apart are combined.

We utilize the simple classification scheme outlined in McFarlane et al. (2013) to designate each cloud layer as belonging to a specific cloud type (Table 2). This simple classification scheme may not necessarily correspond to the meteorological definition of each cloud type, but it does effectively separate the radiative properties (which are primarily a function of the height and depth of the cloud) among different cloud types. This simple scheme has the added benefit of being easily applied to other observational datasets (e.g., satellite cloud retrievals) as well as model output. Thus our analysis can be replicated on other platforms to compare and contrast results. An example of the time–height variation in the radar data and the cloud-classification scheme for a single day at the Manus site is shown in Fig. 1.

All three active sensors are subject to attenuation from heavier rainfall. Attenuation could potentially cause the retrievals to miss some high-level clouds during periods of heavy rain. As such, we discard all 2-min profiles in which the retrieved rain rate [found via a reflectivity–rain rate (Z–R) relationship] at the base of the lowest cloud was larger than 1 mm h^{-1}, which is a conservative threshold for attenuation at the wavelengths that were used. In periods of rain the base of the cloud mask could also be significantly lower than the actual cloud base because of the misclassification of precipitation droplets as cloud droplets in the ARSCL product. In many of these cases the retrieved cloud base extends all the way to the surface (e.g., Fig. 1b). To test the impact of this possible bias, which could lead to the misclassification of cloud type, we ran a sensitivity experiment in which we artificially adjusted the base of the cloud mask to the value measured by the ceilometer, which is not sensitive to precipitation droplets and therefore more accurately measures the true cloud-base height. We found that the potential low bias in the base of the cloud mask during periods of light rain (<1 mm h^{-1}) was unlikely to significantly affect our results (not shown).

One characteristic of the active remote sensors that needs to be considered is a reduced sensitivity to optically thin high-level clouds during periods of high solar elevation angles. As demonstrated in Comstock et al. (2002), there is an approximately 30% decrease in high cloud frequency detected by the MPL at Nauru during the 6-h period centered on solar noon when the sun is highest in the sky. This decrease is attributed to poor MPL signal-to-noise ratios when the solar background energy is large, increasing the noise. In addition, it is ARM practice to physically cover the lidar telescope during times when the sun is nearly overhead to avoid damaging the receiver. More recent comparisons between the MPL and *Cloud–Aerosol Lidar and Infrared Pathfinder Satellite Observations* (*CALIPSO*; Stephens et al. 2002) confirmed that the fraction of cirrus that is not detected by the MPL during daytime is ~25% for clouds above 10 km (Thorsen et al. 2013). Dupont et al. (2011) showed that almost 50% of situations over the ARM Southern Great Plains (SGP) site feature a signal-to-noise ratio that is too low (smaller than 3) for the MPL to infer cloud properties at higher than 7 km using the Structure of Atmosphere (STRAT; Morille et al. 2007) method during summer daylight periods. These limitations suggest that any reduction in the frequency of occurrence of optically thin high-level clouds near solar noon may result from a sampling bias and thus must be interpreted carefully. Throughout the text we acknowledge results that may be biased as a result of these uncorrectable errors.

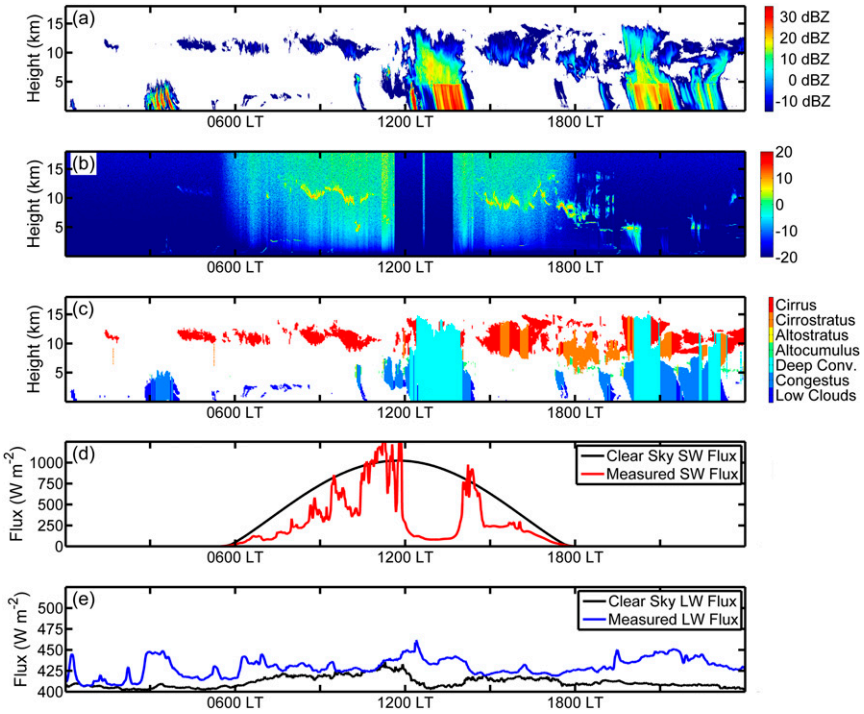

FIG. 1. Time–height evolution of (a) radar reflectivity from KAZR, (b) 10 log10 of the normalized attenuated backscatter from the MPL, (c) the cloud-type classification for each contiguous echo as based on the categories in Table 2, (d) the measured (red line) and estimated (black line) clear-sky SW radiative flux at the surface, and (e) the measured (blue line) and estimated (black line) clear-sky LW radiative flux at the surface. Note that the *y* axes in (d) and (e) are scaled differently by a factor of 10. Data are from the Manus site on 7 Nov 2011, and the LT at the site is given on each *x* axis.

b. Radiative flux analysis

A series of algorithms have been developed that collectively have been termed the radiative flux analysis (Long and Ackerman 2000; Long and Turner 2008). The process uses the time series of measured surface irradiances to look for periods that have the magnitude and temporal variability characteristics that are typical of cloud-free (i.e., clear) skies. The detected clear-sky data are used to empirically fit appropriate functions, the fit coefficients are interpolated for cloudy periods, and then continuous estimates of clear-sky irradiances are produced. The resultant clear-sky estimates are used along with the measured irradiances to infer CRE and effective SW and LW transmissivity.

We define SW or LW CRE as the measured irradiance during cloudy periods minus the estimated clear-sky irradiance. A positive CRE thus corresponds to an increase of radiative energy input at the surface. We define conditional CRE to be the magnitude of the change in SW or LW radiative flux when a given cloud type is present as the lowest cloud layer in the column. When more than one cloud type is present in the column it is not possible to separate the radiative impact of each type. We only focus on the lowest cloud in the column because lower clouds typically have a larger and more direct impact on downwelling SW radiation reaching the surface. The mean CRE describes the average radiative impact for each cloud type (i.e., the frequency at which it occurs as the lowest cloud in the column multiplied by its conditional CRE). We use the term *aggregate CRE* to describe the mean CRE summed over all types of clouds. In addition to CREs, we also calculate the effective SW cloud transmissivity, defined as the ratio of the cloudy SW flux over the clear-sky SW flux. The SW transmissivity indicates the fraction of equivalent clear-sky SW fluxes while removing the dependence on solar zenith angle that is inherent in the SW CRE values.

c. ENSO indices and wet/dry-season classification

ENSO phases for the Manus and Nauru sites are determined from the oceanic Niño index (ONI), which is based on SST anomalies in the Niño-3.4 region relative to a moving 30-yr base period. (Data were obtained online on 13 May 2014 at http://www.cpc.ncep.noaa.gov/products/analysis_monitoring/ensostuff/ensoyears.shtml;

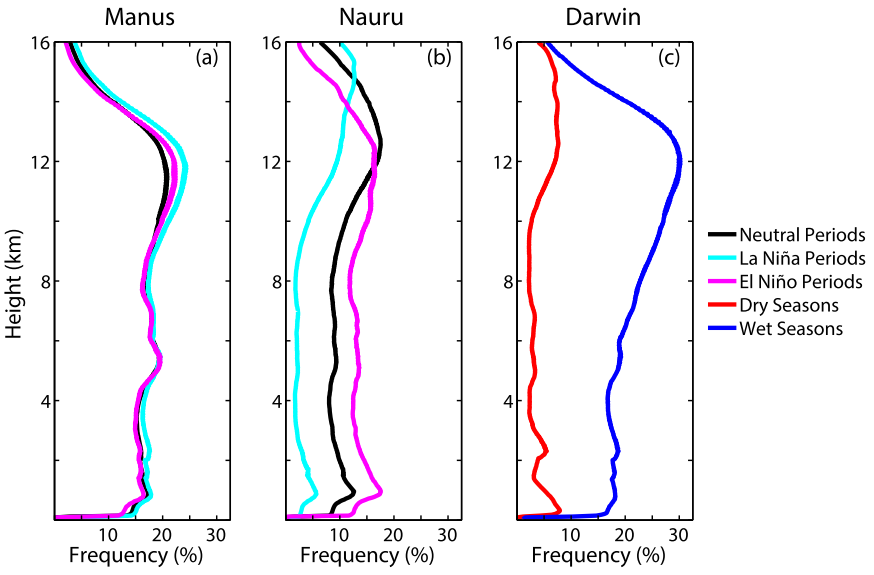

FIG. 2. Frequency distributions of the detection of hydrometeors, both cloud and precipitation particles, by either the radar or lidar at (a) Manus, (b) Nauru, and (c) Darwin. Profiles are separated for neutral (black lines), La Niña (cyan lines), and El Niño (magenta lines) conditions for Manus and Nauru and by dry (red line) and wet (blue line) seasons for Darwin.

see Barnston et al. 1997). We use an ONI threshold of +0.5°C and −0.5°C to classify El Niño and La Niña events, respectively. Time periods with an ONI amplitude that is smaller than 0.5°C are considered to be ENSO neutral. Wet and dry seasons at the Darwin site are separated using an empirical method that is based on the surface radiation measurements. We examine the number of occurrences of daily detected clear-sky data that satisfy the criteria for daily fitting for the Long and Ackerman (2000) algorithm and look for an abrupt change in the frequency of clear-sky data to define the beginning/end of the wet/dry seasons. Our empirical approach to determine the transition between wet and dry seasons agrees well with an objectively defined method (Pope et al. 2009). In general, the dry season runs from roughly May through October and the wet season goes from November through April.

3. Results

a. *Vertical profiles of cloudiness and mean diurnal cycles*

Two distinct modes appear in the vertical profile of hydrometeor frequency (number of cloudy samples/number of total samples) at all three sites from 1 to 2 km and near 12 km (Fig. 2). At Manus there is an additional midlevel cloudiness mode from 4 to 6 km, creating the distinct trimodal structure observed by Johnson et al. (1999). During suppressed cloudiness periods—that is, under La Niña conditions at Nauru (cyan line in Fig. 2b) and during the dry seasons at Darwin (red line in Fig. 2c)—hydrometeor frequency decreases at all levels. The vertical profile of hydrometeor frequency at Manus is not affected by ENSO variability (Fig. 2a). During wet seasons at Darwin (blue line in Fig. 2c) there is an abundance of clouds above 5 km, which is indicative of frequent deep convective clouds and their associated cirrostratus and cirrus remnants. Cirrus clouds over Darwin during the dry season may be more synoptically driven and do not necessarily result from deep convection.

We show the frequency of each cloud type across the diurnal cycle for each individual site in Figs. 3–5. At Manus there is a sizeable diurnal variation in several of the cloud types (Fig. 3). Evidence for the coupling of solar heating and the formation of low clouds, which are primarily shallow cumulus, can be seen in the diurnal cycle of low-cloud frequency (red bars in Fig. 3). Consistent with boundary layer convective clouds that are generated as a result of solar heating, the peak frequency of low clouds occurs at or just after 1200 LT. Deeper convective elements such as cumulus congestus and deep convection peak 2–4 h after the maximum frequency of low clouds. This could be evidence of a shallow-to-deep convective transition, although more evidence is needed to support this hypothesis. Cirrus clouds, which are the most frequent cloud type across the diurnal cycle, increase in frequency starting at 1200 LT and have a peak frequency a few hours after the peak

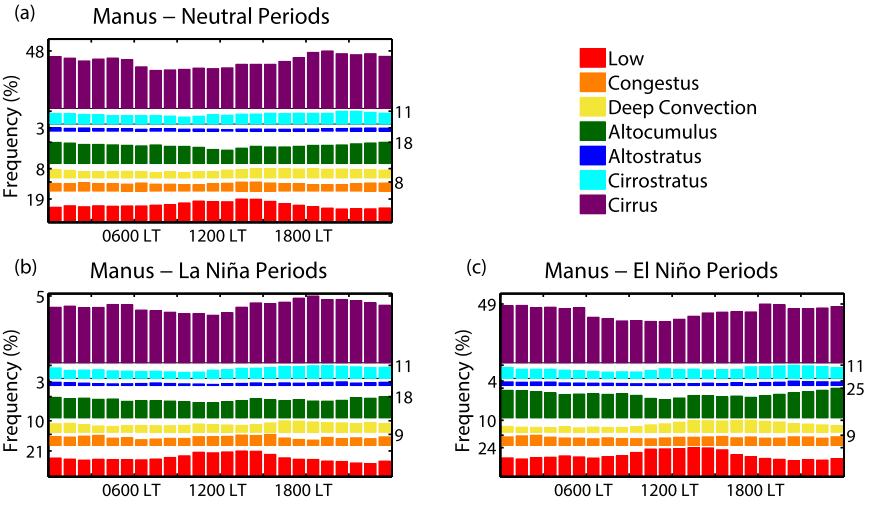

FIG. 3. Mean frequency of occurrence of each cloud type across the diurnal cycle (*x* axis) during (a) neutral, (b) La Niña, and (c) El Niño conditions at Manus. The maximum frequency of each cloud type across the diurnal cycle is given on the *y* axis of each plot. Because multilayer clouds are often present, the total frequency at any given time can add up to greater than 100%.

in convective clouds. The frequency of cirrus clouds remains roughly constant until sunrise. The diurnal cycle in cirrus clouds may be a result of the aforementioned sampling bias of the MPL. Midlevel altocumulus and altostratus clouds at Manus have a smaller-amplitude diurnal cycle than the more convective cloud types. Consistent with the results shown in Fig. 2, there is not a large difference in the diurnal cycle of cloud frequency across the three ENSO phases at Manus.

In contrast to Manus, large variability across ENSO phases can be seen in the data from Nauru (Fig. 4). During neutral and El Niño periods the diurnal cycle at Nauru resembles that observed at Manus. Although it is noisier because there are fewer samples, the diurnal cycle during El Niño periods shows evidence of a potential shallow-to-deep convective transition during the afternoon. There is a clear suppression of midlevel clouds and deeper convective elements during La Niña periods (Fig. 4b). This is likely due to a drying of the troposphere forced by large-scale subsidence as the downward branch of the Walker circulation moves closer to Nauru during La Niña periods (Wang et al. 1999; Wang 2002; Chen et al. 2002). Despite the lack of deeper clouds there is still a small-amplitude diurnal cycle in low clouds and a large-amplitude diurnal cycle in cirrus clouds during La Niña periods. The diurnal minimum of cirrus clouds at 1200 LT is almost certainly a sampling bias, however, given previous work

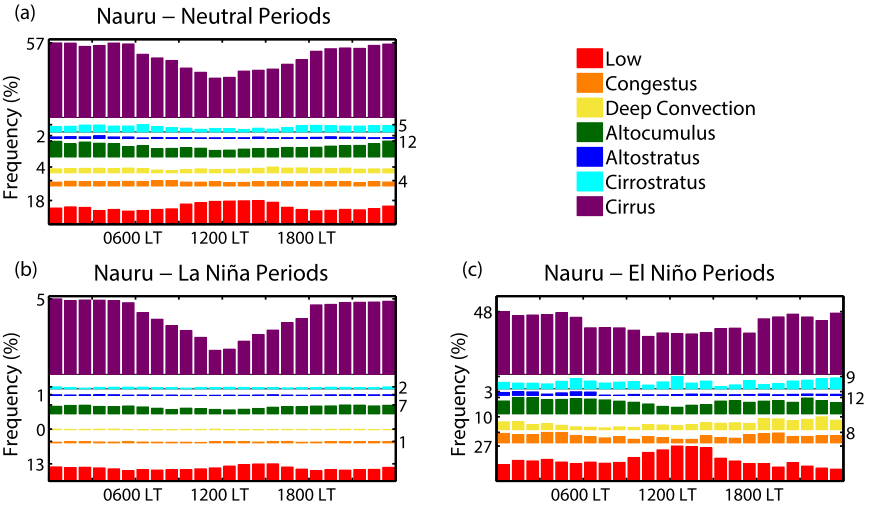

FIG. 4. As in Fig. 3, but at Nauru.

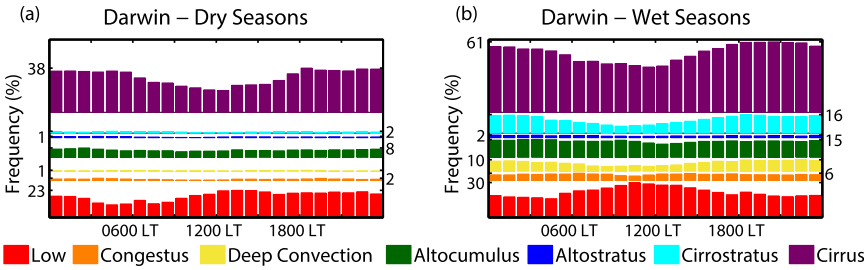

FIG. 5. Similar to Fig. 3, but during the (a) dry and (b) wet seasons at Darwin.

that showed cirrus clouds to be present throughout the day even during dry periods (Comstock et al. 2002; Thorsen et al. 2013). Given the lack of deep convection that could transport surface moisture into the upper parts of the troposphere, the cirrus clouds present over Nauru during La Niña periods are likely not due to local convection.

The lack of midlevel clouds and deeper convective elements is also a dominant signal during the dry seasons at Darwin (Fig. 5a). Smaller-amplitude diurnal cycles are still present in low and cirrus clouds, albeit with lower frequencies, but deep convection as well as cumulus congestus, altostratus, and cirrostratus clouds are rarely present during the dry season. This is consistent with a dry environment that is inhospitable to deeper convective overturning. By contrast, all cloud types are present during the wet seasons (Fig. 5b). The relationship between low clouds and solar forcing and the shallow-to-deep convective transition are both evident during the wet season. Cirrostratus clouds are also abundant during the wet season at Darwin, consistent with the thick layer of high-level clouds over Darwin that is shown in Fig. 2c.

The amplitude of the wet-season diurnal cycle at Darwin (Fig. 5b) is the largest of any of the sites or regimes examined. This is likely due in part to the larger land area surrounding the Darwin site (which is on the edge of a large continent) when compared with the smaller island sizes of Manus ($\sim$2000 km^2) and Nauru ($\sim$20 km^2). Because the diurnal cycle of tropical convection is directly tied to surface heating and diurnal variations in surface convergence from onshore/offshore sea/land breezes (e.g., Biasutti et al. 2012), it follows that the larger landmass at the Darwin site could drive stronger onshore flows and generate more surface instability. This would in turn lead to the larger-amplitude diurnal cycle that is observed. Total land area could also explain why the smallest-amplitude diurnal cycles were observed at the Nauru site. In general the patterns apparent in the diurnal cycle of cloud frequency for all cloud types at each of the three sites are consistent with the existing literature for tropical environments (e.g., Chen and Houze 1997; Soden 2000; Nesbitt and Zipser 2003; Tian et al. 2004; Biasutti et al. 2012). This consistency lends confidence that our simple cloud-type classification system is performing as expected and that the undersampling of cirrus clouds at high solar elevation angles is not significantly affecting our results for total cloud frequency.

b. *Bulk cloud radiative effects*

The total cloudiness and relative frequency of each cloud type across ENSO phases and monsoon seasons affect the aggregate CRE for each time and place. The mean aggregate SW CRE and LW CRE measured at the surface are given in Table 3. Manus has the largest mean aggregate SW CRE (-94.7 W m^{-2}), owing primarily to the large cloud fractions that were observed across all ENSO phases. Data from Nauru reflect the strong ENSO-driven variability. The mean aggregate SW CRE during La Niña periods (-45.9 W m^{-2}) is half that measured during El Niño periods (-92.3 W m^{-2}). A similar signal is seen during the dry seasons at Darwin, where the mean aggregate SW CRE (-23.5 W m^{-2}) is only 25% of that during wet seasons (-95.0 W m^{-2}). Consistent with tropical environments with a strong background LW flux due to high humidity, LW CREs are on average smaller than SW CREs by a factor of 5.

The radiative characteristics of each cloud type at each site are given in Table 4. For this analysis we average values across all ENSO phases and monsoon seasons. Comparing the radiative effects in this way allows us to consider the differences and similarities for a given cloud type across the three TWP sites. The mean SW transmissivity for a given cloud type varies little among the three sites. For example, deep convective clouds have a SW transmissivity that ranges between 0.16 and 0.19 across all three sites. In a similar way, cumulus congestus and cirrus clouds have ranges of 0.33–0.36 and 0.78–0.83, respectively. This is expected given that we define each cloud type on the basis of a restricted range of cloud-base, cloud-top, and cloud-depth values (Table 2). There is still room for the clouds to express

TABLE 3. Mean downwelling SW radiative flux (SWdn), inferred clear-sky SW radiative flux (CSWdn), aggregate SW cloud radiative effect (SW CRE; SWdn − CSWdn), downwelling LW radiative flux (LWdn), inferred clear-sky LW radiative flux (CLWdn), and aggregate LW cloud radiative effect (LW CRE; LWdn − CLWdn) at all three sites. All values are in watts per meter squared and are averaged across the diurnal cycle.

	SWdn	CSWdn	SW CRE	LWdn	CLWdn	LW CRE
			Manus			
All data	205.1	299.8	−94.7	423.5	408.2	15.3
El Niño periods	200.2	302.9	−102.4	423.9	407.6	16.3
Neutral periods	199.5	294.0	−94.4	424.3	408.8	15.5
La Niña periods	214.4	304.6	−90.2	422.3	407.8	14.5
			Nauru			
All data	237.7	302.1	−64.4	420.6	408.5	12.2
El Niño periods	211.9	304.2	−92.3	429.1	414.2	15.0
Neutral periods	229.2	297.9	−68.7	422.9	410.0	12.9
La Niña periods	259.8	305.6	−45.9	413.8	403.8	10.0
			Darwin			
All data	232.4	293.4	−61.0	407.0	394.6	12.4
Dry seasons	239.1	262.7	−23.5	384.2	376.4	7.8
Wet seasons	226.5	321.5	−95.0	427.9	411.5	16.4

some natural variability between sites through variations in cloud microphysics, however. The narrow range of SW transmissivities indicates that this variability is small and that clouds of a given type behave similarly at each of the three sites. The radiative properties of a given cloud type at one site across ENSO phases or monsoon seasons are also roughly constant (not shown). Given that the variance in SW radiative properties is small, we can conclude that, to first order, variations in the magnitude of the aggregate SW CRE across the TWP sites and across ENSO phases or monsoon seasons at a particular site are primarily forced by changes to the absolute and relative frequency of each cloud type rather than by differences in the radiative properties of a given cloud type across the three sites.

c. *Diurnal cycles of cloud radiative effects by cloud type*

Examining the conditional and mean CRE of each cloud type allows us to see which clouds are having the

TABLE 4. Mean frequency, frequency as the lowest cloud layer in the column, conditional SW transmissivity (SW Trn), conditional SW cloud radiative effect (SW CRE), and conditional LW cloud radiative effect (LW CRE) for each cloud type at each site. All values are averaged across the diurnal cycle.

		Frequency (%)	Frequency as lowest cloud (%)	SW Trn	SW CRE ($W m^{-2}$)	LW CRE ($W m^{-2}$)
Low	Manus	15.9	23.4	0.52	−336.5	27.0
	Nauru	12.2	20.9	0.58	−291.4	26.2
	Darwin	21.1	31.1	0.63	−261.1	23.3
Congestus	Manus	5.8	8.5	0.36	−432.7	30.8
	Nauru	2.1	3.6	0.33	−445.1	30.5
	Darwin	3.7	5.4	0.33	−451.9	34.3
Deep convection	Manus	6.7	9.9	0.19	−539.5	33.1
	Nauru	2.0	3.4	0.17	−576.1	31.0
	Darwin	5.7	8.4	0.16	−560.2	34.9
Altocumulus	Manus	11.3	16.6	0.68	−193.5	16.9
	Nauru	5.0	8.6	0.70	−178.3	14.6
	Darwin	7.6	11.2	0.69	−197.6	18.4
Altostratus	Manus	1.2	1.8	0.58	−256.7	20.1
	Nauru	0.4	0.7	0.55	−292.3	19.3
	Darwin	0.8	1.1	0.56	−271.9	22.9
Cirrostratus	Manus	4.1	6.1	0.48	−337.3	18.0
	Nauru	1.4	2.3	0.50	−329.8	14.8
	Darwin	4.3	6.3	0.43	−361.9	20.6
Cirrus	Manus	22.9	33.7	0.78	−129.3	7.4
	Nauru	35.1	60.4	0.83	−100.1	5.3
	Darwin	24.7	36.5	0.82	−114.0	8.4

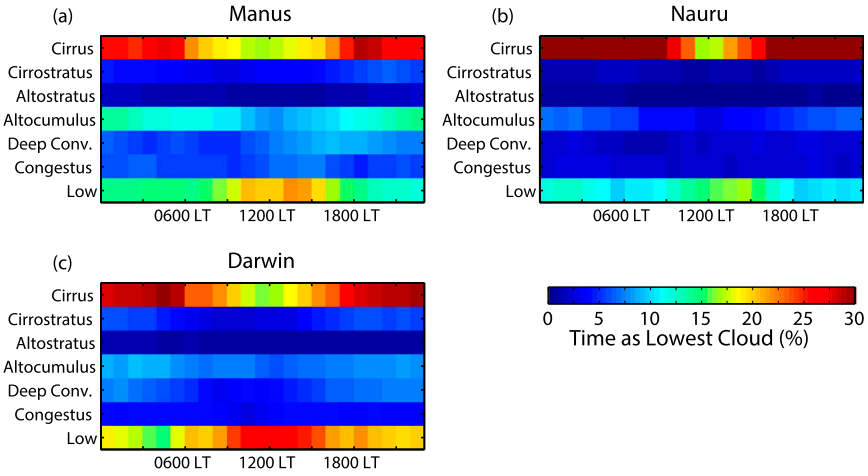

FIG. 6. Percent of time that each cloud type (y axis) is the lowest cloud in the column as a function of the diurnal cycle (x axis) at (a) Manus, (b) Nauru, and (c) Darwin.

greatest impact on the surface energy budget. This analysis builds on the cloud-type CRE analysis in McFarlane et al. (2013) but is expanded to include the diurnal cycle of CREs. The shortwave radiative properties of each cloud type across the diurnal cycle are shown in Figs. 7–9, described below. In general the patterns observed at the three sites are similar, and therefore our analysis can be generically interpreted as pertaining to all sites. Data in this analysis are accumulated across all ENSO phases at Manus and Nauru and across both the wet and dry seasons at Darwin.

In Fig. 6 we show the percent of time that a given cloud type is the lowest cloud in the column as a function of the diurnal cycle. At all three sites the lowest cloud in the column across the diurnal cycle is most often either low clouds, which are at a maximum in the early afternoon, or cirrus clouds, which occur most frequently in the early morning and late afternoon. This pattern, which is likely to some degree attributable to the aforementioned sampling biases of the MPL, is particularly clear at Nauru and Darwin. At these two sites midlevel clouds occur less often than at Manus, reflecting the impact of the dry seasons at Darwin and periods with La Niña conditions at Nauru (Figs. 2, 4, and 5). At Manus, deep convection and cumulus congestus clouds both have a small-amplitude diurnal cycle with peak frequencies occurring in the afternoon (Fig. 6a).

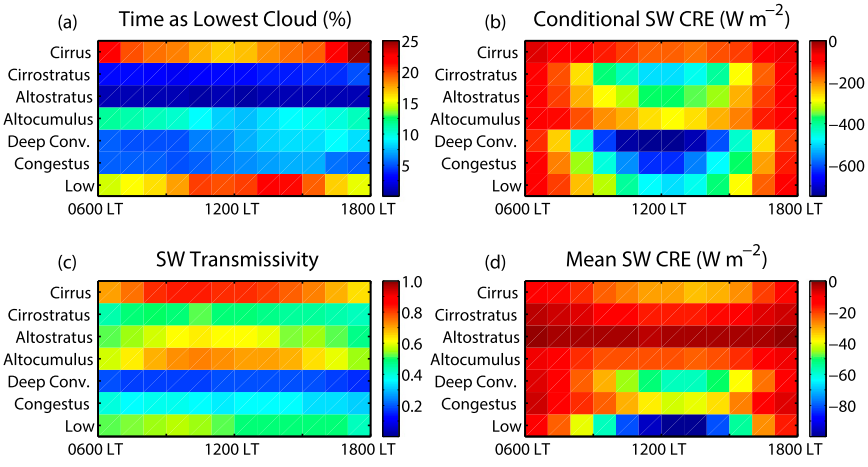

FIG. 7. (a) Percent of time that each cloud type is the lowest cloud in the column. (b) Change in the downwelling SW radiative flux when a cloud is present. (c) Ratio of the measured and inferred clear-sky downwelling SW radiative flux when a cloud is present. (d) Mean SW CRE (frequency of occurrence times the conditional SW CRE). Data are from the Manus site and are divided into individual cloud types (y axis) and are shown as a function of the diurnal cycle (x axis) from roughly sunrise to sunset.

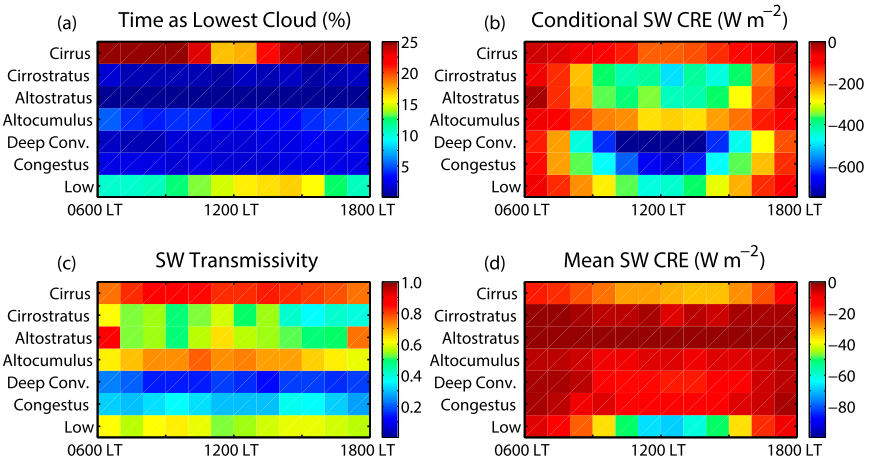

FIG. 8. As in Fig. 7, but for Nauru.

The plots of conditional SW CRE (Figs. 7b, 8b, and 9b) show the reduction in downwelling SW flux when a given cloud type is present as the lowest cloud in the column at a particular time of day. The SW transmissivity plots (Figs. 7c–9c) similarly show the fraction of downwelling SW flux that is able to penetrate through the cloud when present. The SW transmissivity removes the dependence on solar elevation angle that is evident in the diurnal cycle of SW CRE. Vertically extensive deep convection and cumulus congestus clouds have the lowest SW transmissivity values, and therefore they also have the largest-magnitude conditional SW CRE. Cirrus clouds allow the most downwelling SW radiative flux to penetrate through to the surface. The SW transmissivities for cirrus clouds at all three sites range from 0.8 to 0.9 for most of the day but are roughly 0.7 during the early morning and late afternoon. This is likely due to increased slant paths through the cirrus layers. Because the SW transmissivity for each cloud type exhibits a limited range across the diurnal cycle, we can conclude that the diurnal cycle in conditional SW CREs for a given cloud type primarily reflects the diurnal cycle of solar irradiance. Clouds present at 1200 LT have more incoming SW radiation to reflect and absorb and thus have a larger conditional SW CRE than do clouds that form in the early morning or late afternoon.

The mean SW radiative impact of each cloud type is a balance involving how frequently they occur as the lowest cloud in the column, when they occur with respect to the maximum downwelling SW fluxes, and how much radiation they can reflect and absorb when present. These properties are expressed in combination as the mean SW CRE for each cloud type across the diurnal cycle (Figs. 7d, 8d, and 9d). Deep convective clouds have larger conditional SW CRE, but low clouds have larger mean SW CRE because of their relatively higher frequencies. At all three sites low clouds have the largest mean surface

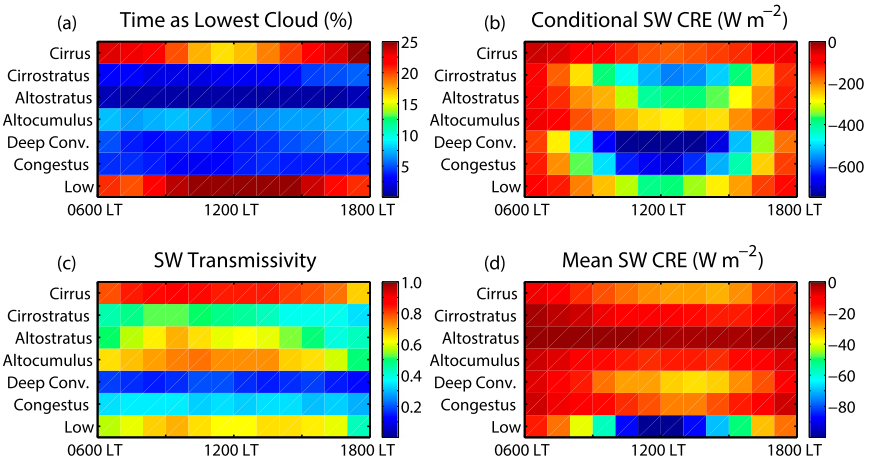

FIG. 9. As in Fig. 7, but for Darwin.

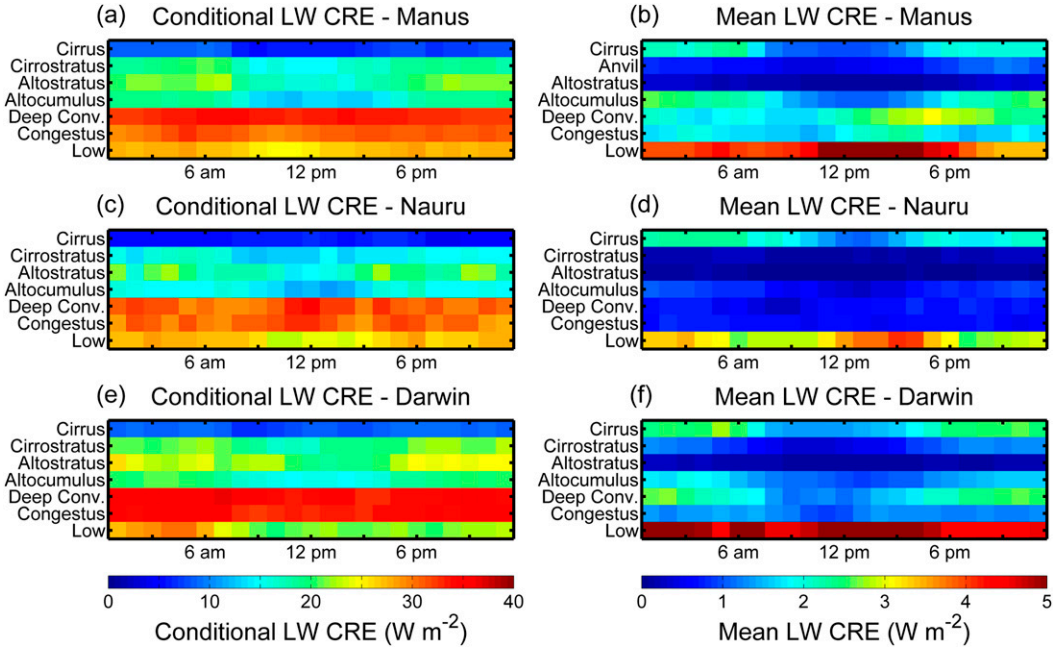

FIG. 10. (left) Change in the downwelling LW radiative flux when a cloud is present, and (right) the mean LW CRE (frequency of occurrence times the conditional LW CRE). CREs are divided for individual cloud types (*y* axis) and are shown as a function of the diurnal cycle (*x* axis) at (a),(b) Manus, (c),(d) Nauru, and (e),(f) Darwin. Note that the color scales in the two columns are scaled differently by a factor of 8.

SW CRE and altostratus have the smallest. This result agrees with several previous studies looking at CRE on both the TOA (Hartmann et al. 1992; Chen et al. 2000) and surface energy budgets (Mace et al. 2006).

The conditional LW CRE for each cloud type (left column of Fig. 10) is roughly constant across the diurnal cycle and is primarily a function of the height (and associated ambient temperature at cloud base) of each cloud type. Clouds with lower bases (low, cumulus congestus, and deep convective clouds) have a larger conditional LW CRE. As with the SW CRE, the mean LW CRE (right column of Fig. 10) is a combination of the frequency of each cloud type and its radiative properties. The mean LW CRE is largest for low clouds at all three sites. Although they have a small conditional LW CRE, cirrus clouds have some impact on the mean LW radiative flux reaching the surface because of how often they are present as the lowest cloud in the column (Fig. 6). As with the SW CRE, diurnal variability in the mean LW CRE for a given cloud type is primarily driven by variations in frequency across the diurnal cycle.

d. Sensitivity to frequency and the timing of the diurnal cycle

Given that models often fail to replicate the absolute frequency and the diurnal cycle of frequency for some types of clouds, it follows that these errors will lead to biases in their simulated aggregate SW and LW CRE. Klein et al. (2013) compared the ensemble mean distributions of cloudiness by cloud type from the Cloud Feedback Model Intercomparison Project 1 (CFMIP1) and CFMIP2 simulations with International Satellite Cloud Climatology Project observations. They found typical cloud frequency biases on the order of 5%–10%, with larger biases preferentially occurring in optically thin and low clouds (their Figs. 2 and 3). We can quantify the sensitivity to frequency errors of this magnitude by perturbing the observed frequencies of each cloud type, essentially artificially generating biases in frequency for each cloud type and then calculating the change in the aggregate SW and LW CRE across all cloud types. This analysis will demonstrate how model errors in the absolute frequency of each cloud type could affect their simulated surface radiation budget.

In Fig. 11 we show the change in the aggregate (summed over all cloud types and across the diurnal cycle) SW CRE that occurs when the relative frequency of a given cloud type is changed by ±10%. Another way to think of this analysis is to ask, If a model has a ±10% bias in the frequency of a particular cloud type, how much is the SW CRE likely to be over- or underestimated? For some cloud types with absolute frequencies lower than 10% we stop the sensitivity analysis

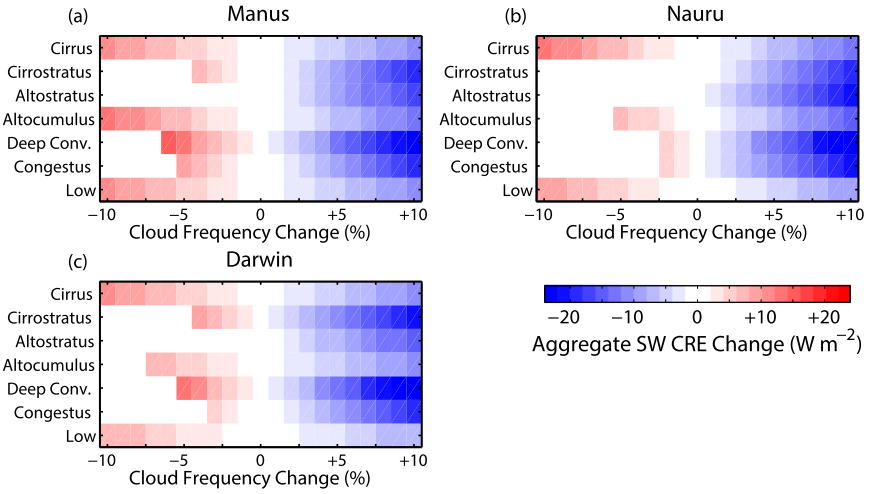

FIG. 11. Change in the aggregate SW CRE that results from changes in the frequency (*x* axis) of each cloud type (*y* axis) at (a) Manus, (b) Nauru, and (c) Darwin. Note that the color scale range is larger than that in Figs. 12 and 13 by a factor of 6.

when cloud frequency goes to 0%. For example, at Manus cumulus congestus clouds occur roughly 5% of the time on average, and so the maximum negative frequency error that can be imposed is −5% (Fig. 11a).

Errors in the absolute frequency of deeper convective clouds produce the largest biases in the aggregate SW CRE (Fig. 11). Overestimating the absolute frequency of deep convective clouds by +10% leads to errors of roughly $-20\,\mathrm{W\,m^{-2}}$ in the aggregate SW CRE at Manus. This is more than 20% of the mean SW CRE ($-94.7\,\mathrm{W\,m^{-2}}$; Table 3). Errors in the absolute frequency of other cloud types have a relatively smaller impact on the aggregate SW CRE. In other words, a model that misses the absolute frequency of deep convection or cumulus congestus by +10% will have a larger bias in the surface energy budget than will a model that overestimates the absolute frequency of low clouds by +10%. These results demonstrate that capturing the absolute frequency of optically thick clouds such as deep convection and cumulus congestus is important to reducing model errors in the aggregate SW CRE.

Changes in the aggregate LW CRE are smaller by a factor of ~5 than changes in the aggregate SW CRE for similar biases in absolute cloud frequency (Fig. 12). The largest shifts in aggregate LW CRE are due to over- or underestimation of clouds with low bases. The aggregate

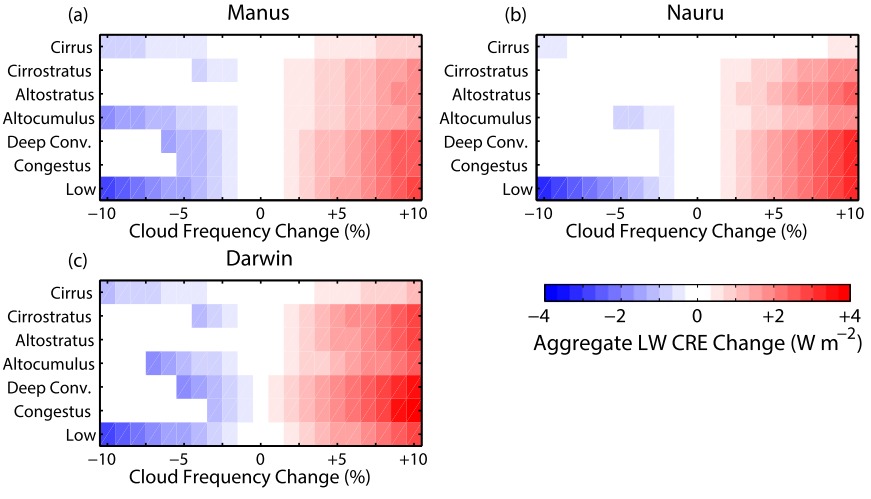

FIG. 12. Change in the aggregate LW CRE that results from errors in the frequency (*x* axis) of each cloud type (*y* axis) at (a) Manus, (b) Nauru, and (c) Darwin. Note that the color scale range is smaller than that in Fig. 11 by a factor of 6.

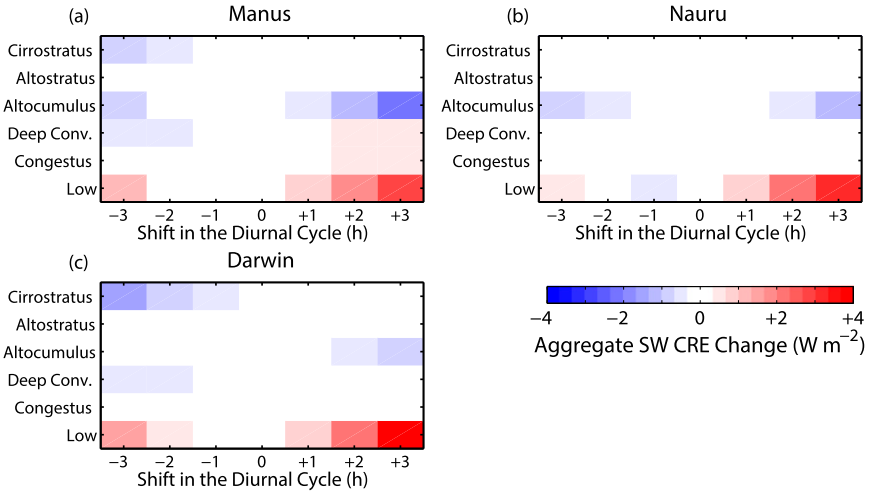

FIG. 13. Change in the aggregate SW CRE that results from shifts in the diurnal cycle of cloud frequency (x axis) of each cloud type (y axis) at (a) Manus, (b) Nauru, and (c) Darwin. The diurnal cycle in frequency for each cloud type is shifted by up to 3 h earlier (negative values) or 3 h later (positive values) than the observed diurnal cycle. Note that the color scale range is smaller than in Fig. 11 by a factor of 6.

LW CRE is largely insensitive to small biases in the frequency of cirrostratus or cirrus clouds. Combined together these results indicate that at Manus, for example, a 10% overestimation of deep convection leads to a roughly $-15\,\mathrm{W\,m^{-2}}$ net (aggregate SW CRE + aggregate LW CRE) error in the surface radiation budget.

Models of all sizes and resolutions struggle to replicate not only the absolute frequency of each cloud type but also the timing of occurrence across the diurnal cycle. For example, in their study of the diurnal cycle of precipitation in the "Maritime Continent," Arakawa and Kitoh (2005) showed that their GCM had a peak frequency of deep convection occurring 2–3 h too early relative to observations. Sato et al. (2009) similarly found a resolution-dependent diurnal cycle bias that is 2–3 h too late. Because SW CRE is a function of the background solar irradiance, errors in the timing of the diurnal cycle of cloud frequency will directly lead to errors in the aggregate SW CRE simulated in a given model. We can shift the diurnal cycle of cloud frequency of a given cloud type to test the sensitivity to timing. In Fig. 13 we show the change in aggregate SW CRE that results when the diurnal cycle in cloud frequency for a given cloud type is shifted earlier (negative values) and later (positive values) in time by ±3 h. We exclude cirrus clouds from this analysis because the aforementioned sampling bias near solar noon creates an anomalously large sensitivity to the timing of the diurnal cycle. Small errors in the timing of low clouds can lead to a reduction in the aggregate SW CRE by up to $+3\,\mathrm{W\,m^{-2}}$. The shift toward a smaller CRE when the timing of low clouds is shifted in either direction reflects the fact that peak low-cloud frequency occurs near solar noon. None of the other cloud types show significant sensitivity to the timing of the diurnal cycle. This is not surprising since their diurnal amplitudes are small relative to that of low clouds (Fig. 6). Shifts in the timing of the diurnal cycle of cloud frequency have a much smaller impact on the aggregate SW CRE relative to biases in the absolute frequency of each cloud type.

4. Conclusions

Long-term measurements of the surface SW and LW radiation budgets are combined with a unique cloud-frequency dataset to quantify CRE at the three ARM sites in the TWP. This work builds on McFarlane et al. (2013), who examined bulk CRE in the TWP datasets. The novel contribution of our analysis is that we break CRE down by cloud type and across the diurnal cycle. We are also the first to quantify aggregate SW and LW CRE errors that would result from model biases in the frequency of clouds or the timing of the diurnal cycle. Our four primary findings are the following:

1) Most of the variability in aggregate SW and LW CRE among the three sites and across ENSO phases or monsoon seasons at a particular site is driven by variations in the relative and absolute frequency of each cloud type. The radiative properties of each cloud type (i.e., SW transmissivity and LW CRE) are roughly constant between sites and across the diurnal cycle.
2) Although deeper clouds (cumulus congestus and deep convection) have larger conditional SW CREs,

they have a smaller mean SW CRE relative to low clouds because they only occur infrequently.

3) Small (±10%) biases in the absolute frequency of deep convection and cumulus congestus clouds will lead to large ($\pm 20\,W\,m^{-2}$) errors in the aggregate SW CRE. Similar sized biases in the frequency of low clouds only lead to small errors in the aggregate SW CRE.
4) Errors in the absolute frequency of each cloud type lead to larger changes in the aggregate SW CRE in comparison with errors in the timing of the diurnal cycle of cloud frequency.

These results point toward a system in which the modulation of the surface radiation budget by tropical clouds is primarily controlled by cloud frequency. This is akin to the well-established fact that the climatological behavior of precipitation accumulation is dominated by variations in precipitation frequency rather than intensity (e.g., Dai 2001; Schumacher and Houze 2006; Zipser et al. 2006; Biasutti et al. 2012; Biasutti and Yuter 2013). Likewise, the surface radiation budget is most sensitive to the frequency of clouds as opposed to variations in cloud radiative properties (Dhuria and Kyle 1990; Wielicki et al. 2002). This sensitivity was previously documented in the midlatitudes using data from the SGP ARM site (Mace et al. 2006). They showed quantitatively that cloud-frequency variability was more important than cloud microphysical variability in terms of the net effect of clouds on the midlatitude surface energy budget. Our quantitative analysis extends this pattern to the tropics and highlights the importance of low clouds on the tropical surface energy budget. The importance of low clouds has been shown in several previous studies in the tropics (Hartmann et al. 1992; Chen et al. 2000) and extratropics (Tselioudis and Rossow 2006; Govekar et al. 2011).

Previous work has shown that the cloud regimes and radiative characteristics at the TWP ARM sites are broadly representative of the global tropics (e.g., Jakob et al. 2005; Long et al. 2013), and therefore our results may be applicable in a much larger context of tropical cloudiness. More work is needed to confirm the representativeness of our findings. The patterns, frequencies, and relationships that are documented in this study provide robust targets for future modeling efforts of cloud effects on the tropical surface radiation budget. Our simple classification scheme for identifying cloud types could readily be translated to be applicable for a wide range of model types. Using our basic framework for separating cloud radiative effects diurnally and by cloud type, models could be evaluated on their ability to accurately simulate the bulk surface energy budget as well as the absolute and relative frequency of different types of clouds and how each cloud type modifies SW and LW fluxes at the surface. Long-term simulations that focus on intraseasonal-to-interannual variability in the tropics could also compare their output with our results showing the impact of ENSO and monsoon-related variability on these three tropical sites.

Acknowledgments. Zhe Feng, Julia Flaherty, Samson Hagos, and Laura Riihimaki provided valuable feedback on this work. This research is based on work that was supported by the U.S. Department of Energy, Office of Science, Biological and Environmental Research, as part of the Atmospheric System Research (ASR) Program and used data from the ARM Climate Research Facility, which is a DOE Office of Science user facility. The Pacific Northwest National Laboratory is operated for DOE by Battelle Memorial Institute under Contract DE-AC06-76RLO 1830.

REFERENCES

Arakawa, O., and A. Kitoh, 2005: Rainfall diurnal variation over the Indonesian Maritime Continent simulated by 20 km-mesh GCM. *SOLA,* **1,** 109–112, doi:10.2151/sola.2005-029.

Arking, A., 1991: The radiative effects of clouds and their impact on climate. *Bull. Amer. Meteor. Soc.,* **72,** 795–813, doi:10.1175/1520-0477(1991)072<0795:TREOCA>2.0.CO;2.

Barnston, A. G., M. Chelliah, and S. B. Goldenberg, 1997: Documentation of a highly ENSO-related SST region in the equatorial Pacific. *Atmos.–Ocean,* **35,** 367–383, doi:10.1080/07055900.1997.9649597.

Biasutti, M., and S. E. Yuter, 2013: Observed frequency and intensity of tropical precipitation from instantaneous estimates. *J. Geophys. Res. Atmos.,* **118,** 9534–9551, doi:10.1002/jgrd.50694.

——, ——, C. D. Burleyson, and A. H. Sobel, 2012: Very high resolution rainfall patterns measured by TRMM Precipitation Radar: Seasonal and diurnal cycles. *Climate Dyn.,* **39,** 239–258, doi:10.1007/s00382-011-1146-6.

Cess, R. D., M. Zhang, B. A. Wielicki, D. F. Young, X.-L. Zhou, and Y. Nikitenko, 2001: The influence of the 1998 El Niño upon cloud-radiative forcing over the Pacific warm pool. *J. Climate,* **14,** 2129–2137, doi:10.1175/1520-0442(2001)014<2129:TIOTEN>2.0.CO;2.

Chen, J., B. E. Carlson, and A. D. Del Genio, 2002: Evidence for strengthening of the tropical general circulation in the 1990s. *Science,* **295,** 838–841, doi:10.1126/science.1065835.

Chen, S. S., and R. A. Houze Jr., 1997: Diurnal variation and lifecycle of deep convective systems over the tropical Pacific warm pool. *Quart. J. Roy. Meteor. Soc.,* **123,** 357–388, doi:10.1002/qj.49712353806.

Chen, T., W. B. Rossow, and Y. Zhang, 2000: Radiative effects of cloud-type variations. *J. Climate,* **13,** 264–286, doi:10.1175/1520-0442(2000)013<0264:REOCTV>2.0.CO;2.

Clothiaux, E. E., and Coauthors, 2001: The ARM Millimeter Wave Cloud Radars (MMCRs) and the Active Remote Sensing of Clouds (ARSCL) Value Added Product (VAP). DOE Tech. Memo. ARM VAP-002.1, 56 pp. [Available online at https://www.arm.gov/publications/tech_reports/arm-vap-002-1.pdf.]

Colman, R., 2003: A comparison of climate feedbacks in general circulation models. *Climate Dyn.,* **20,** 865–873, doi:10.1007/s00382-003-0310-z.

Comstock, J. M., T. P. Ackerman, and G. G. Mace, 2002: Ground-based lidar and radar remote sensing of tropical cirrus clouds at Nauru Island: Cloud statistics and radiative impacts. *J. Geophys. Res.,* **107,** 4714, doi:10.1029/2002JD002203.

——, A. Protat, S. A. McFarlane, J. Delanoe, and M. Deng, 2013: Assessment of uncertainty in cloud radiative effects and heating rates through retrieval algorithm differences: Analysis using 3 years of ARM data at Darwin, Australia. *J. Geophys. Res. Atmos.,* **118,** 4549–4571, doi:10.1002/jgrd.50404.

Dai, A., 2001: Global precipitation and thunderstorm frequencies. Part I: Seasonal and interannual variations. *J. Climate,* **14,** 1092–1111, doi:10.1175/1520-0442(2001)014<1092:GPATFP>2.0.CO;2.

——, 2006: Precipitation characteristics in eighteen coupled climate models. *J. Climate,* **19,** 4605–4630, doi:10.1175/JCLI3884.1.

Dhuria, H. L., and H. L. Kyle, 1990: Cloud types and the tropical Earth radiation budget. *J. Climate,* **3,** 1409–1434, doi:10.1175/1520-0442(1990)003<1409:CTATTE>2.0.CO;2.

Dufresne, J.-L., and S. Bony, 2008: An assessment of the primary sources of spread of global warming estimates from coupled atmosphere–ocean models. *J. Climate,* **21,** 5135–5144, doi:10.1175/2008JCLI2239.1.

Dupont, J.-C., M. Haeffelin, Y. Morille, J. M. Comstock, C. Flynn, C. N. Long, C. Sivaraman, and R. K. Newson, 2011: Cloud properties derived from two lidars over the ARM SGP site. *Geophys. Res. Lett.,* **38,** L08814, doi:10.1029/2010GL046274.

Govekar, P. D., C. Jakob, M. J. Reeder, and J. Haynes, 2011: The three-dimensional distribution of clouds around Southern Hemisphere extratropical cyclones. *Geophys. Res. Lett.,* **38,** L21805, doi:10.1029/2011GL049091.

Hartmann, D. L., M. E. Ockert-Bell, and M. L. Michelson, 1992: The effect of cloud type on Earth's energy balance: Global analysis. *J. Climate,* **5,** 1281–1304, doi:10.1175/1520-0442(1992)005<1281:TEOCTO>2.0.CO;2.

Jakob, C., G. Tselioudis, and T. Hume, 2005: The radiative, cloud, and thermodynamic properties of major tropical western Pacific cloud regimes. *J. Climate,* **18,** 1203–1215, doi:10.1175/JCLI3326.1.

Jensen, M. P., and A. D. Del Genio, 2003: Radiative and microphysical characteristics of deep convective systems in the tropical western Pacific. *J. Appl. Meteor.,* **42,** 1234–1254, doi:10.1175/1520-0450(2003)042<1234:RAMCOD>2.0.CO;2.

Johnson, R. H., T. M. Rickenback, S. A. Rutledge, P. E. Ciesielski, and W. H. Schubert, 1999: Trimodal characteristics of tropical convection. *J. Climate,* **12,** 2397–2418, doi:10.1175/1520-0442(1999)012<2397:TCOTC>2.0.CO;2.

Klein, S. A., Y. Zhang, M. D. Zelinka, R. Pincus, J. Boyle, and P. J. Gleckler, 2013: Are climate model simulations of clouds improving? An evaluation using the ISCCP simulator. *J. Geophys. Res. Atmos.,* **118,** 1329–1342, doi:10.1002/jgrd.50141.

Kuang, Z., Y. Jiang, and Y. L. Yung, 1998: Cloud optical thickness variations during 1983–1991: Solar cycle or ENSO? *Geophys. Res. Lett.,* **25,** 1415–1417, doi:10.1029/98GL00471.

Li, J.-L. F., and Coauthors, 2012: An observationally based evaluation of cloud ice water in CMIP3 and CMIP5 GCMs and contemporary reanalyses using contemporary satellite data. *J. Geophys. Res.,* **117,** D16105, doi:10.1029/2012JD017640.

Loeb, N. G., B. A. Wielicki, D. R. Doelling, G. L. Smith, D. F. Keyes, S. Kato, N. Manalo-Smith, and T. Wong, 2009: Toward optimal closure of the Earth's top-of-atmosphere radiation budget. *J. Climate,* **22,** 748–766, doi:10.1175/2008JCLI2637.1.

Long, C. N., and T. P. Ackerman, 2000: Identification of clear skies from broadband pyranometer measurements and calculation of downwelling shortwave cloud effects. *J. Geophys. Res.,* **105,** 15 609–15 626, doi:10.1029/2000JD900077.

——, and D. D. Turner, 2008: A method for continuous estimation of clear-sky downwelling longwave radiative flux developed using ARM surface measurements. *J. Geophys. Res.,* **113,** D18206, doi:10.1029/2008JD009936.

——, and Coauthors, 2013: ARM research in the equatorial western Pacific: A decade and counting. *Bull. Amer. Meteor. Soc.,* **94,** 695–708, doi:10.1175/BAMS-D-11-00137.1.

Mace, G. G., S. Benson, and S. Kato, 2006: Cloud radiative forcing at the Atmospheric Radiation Measurement Program Climate Research Facility: 2. Vertical redistribution of radiant energy by clouds. *J. Geophys. Res.,* **111,** D11S91, doi:10.1029/2005JD005922.

——, Q. Q. Zhang, M. Vaughan, R. Marchand, G. Stephens, C. Trepte, and D. Winker, 2009: A description of hydrometeor layer occurrence statistics derived from the first year of merged *CloudSat* and *CALIPSO* data. *J. Geophys. Res.,* **114,** D00A26, doi:10.1029/2007JD009755.

Mather, J. H., T. P. Ackerman, W. E. Clements, F. J. Barnes, M. D. Ivey, L. D. Hatfield, and R. M. Reynolds, 1998: An atmospheric radiation and cloud station in the tropical western Pacific. *Bull. Amer. Meteor. Soc.,* **79,** 627–642, doi:10.1175/1520-0477(1998)079<0627:AARACS>2.0.CO;2.

McFarlane, S. A., C. N. Long, and D. M. Flynn, 2005: Impact of island-induced clouds on surface measurements: Analysis of the ARM Nauru Island Effect Study data. *J. Appl. Meteor.,* **44,** 1045–1065, doi:10.1175/JAM2241.1.

——, ——, and J. Flaherty, 2013: A climatology of surface radiative effects at the ARM tropical western Pacific sites. *J. Appl. Meteor. Climatol.,* **52,** 996–1013, doi:10.1175/JAMC-D-12-0189.1.

Morille, Y., M. Haeffelin, P. Drobinski, and J. Pelon, 2007: STRAT: An automated algorithm to retrieve the vertical structure of the atmosphere from single-channel lidar data. *J. Atmos. Oceanic Technol.,* **24,** 761–775, doi:10.1175/JTECH2008.1.

Nesbitt, S. W., and E. J. Zipser, 2003: The diurnal cycle of rainfall and convective intensity according to three years of TRMM measurements. *J. Climate,* **16,** 1456–1475, doi:10.1175/1520-0442-16.10.1456.

Pope, M., C. Jakob, and M. J. Reeder, 2009: Regimes of the north Australian wet season. *J. Climate,* **22,** 6699–6715, doi:10.1175/2009JCLI3057.1.

Randall, D., A. Harshvardhan, D. A. Dazlich, and T. G. Corsetti, 1989: Interactions among radiation, convection, and large-scale dynamics in a general circulation model. *J. Atmos. Sci.,* **46,** 1943–1970, doi:10.1175/1520-0469(1989)046<1943:IARCAL>2.0.CO;2.

Sato, T., H. Miura, M. Satoh, Y. N. Takayabu, and Y. Wang, 2009: Diurnal cycle of precipitation in the tropics simulated in a global cloud-resolving model. *J. Climate,* **22,** 4809–4826, doi:10.1175/2009JCLI2890.1.

Schumacher, C., and R. A. Houze Jr., 2006: Stratiform precipitation production over sub-Saharan Africa and the tropical east Atlantic as observed by TRMM. *Quart. J. Roy. Meteor. Soc.,* **132,** 2235–2255, doi:10.1256/qj.05.121.

Slingo, A., and J. M. Slingo, 1988: The response of a general circulation model to cloud longwave radiative forcing. I: Introduction and initial experiments. *Quart. J. Roy. Meteor. Soc.,* **114,** 1027–1062, doi:10.1002/qj.49711448209.

Soden, B. J., 2000: The diurnal cycle of convection, clouds, and water vapor in the tropical upper troposphere. *Geophys. Res. Lett.,* **27,** 2173–2176, doi:10.1029/2000GL011436.

——, and I. M. Held, 2006: An assessment of climate feedbacks in coupled ocean–atmosphere models. *J. Climate,* **19,** 3354–3360, doi:10.1175/JCLI3799.1.

Stephens, G. L., 2005: Cloud feedbacks in the climate system: A critical review. *J. Climate,* **18,** 237–273, doi:10.1175/JCLI-3243.1.

——, and Coauthors, 2002: The *CloudSat* mission and the A-Train: A new dimension of space-based observations of clouds and precipitation. *Bull. Amer. Meteor. Soc.,* **83,** 1771–1790, doi:10.1175/BAMS-83-12-1771.

Stubenrauch, C. J., and Coauthors, 2013: Assessment of global cloud datasets from satellites: Project and database initiated by the GEWEX Radiation Panel. *Bull. Amer. Meteor. Soc.,* **94,** 1031–1049, doi:10.1175/BAMS-D-12-00117.1.

Su, H., and Coauthors, 2013: Diagnosis of regime-dependent cloud simulation errors in CMIP5 models using A-Train satellite observations and reanalysis data. *J. Geophys. Res.,* **118,** 2762–2780, doi:10.1029/2012JD018575.

Thorsen, T. J., Q. Fu, J. M. Comstock, C. Sivaraman, M. A. Vaughan, D. M. Winker, and D. D. Turner, 2013: Macrophysical properties of tropical cirrus clouds from the *CALIPSO* satellite and from ground-based micropulse and Raman lidars. *J. Geophys. Res. Atmos.,* **118,** 9209–9220, doi:10.1002/jgrd.50691.

Tian, B., B. J. Soden, and X. Wu, 2004: Diurnal cycle of convection, clouds, and water vapor in the tropical upper troposphere: Satellites versus a general circulation model. *J. Geophys. Res.,* **109,** D10101, doi:10.1029/2003JD004117.

Tselioudis, G., and W. B. Rossow, 2006: Climate feedback implied by observed radiation and precipitation changes with midlatitude storm strength and frequency. *Geophys. Res. Lett.,* **33,** L02704, doi:10.1029/2005GL024513.

Wang, C., 2002: Atmospheric circulation cells associated with the El Niño–Southern Oscillation. *J. Climate,* **15,** 399–419, doi:10.1175/1520-0442(2002)015<0399:ACCAWT>2.0.CO;2.

——, R. H. Weisberg, and J. I. Virmani, 1999: Western Pacific interannual variability associated with the El Niño–Southern Oscillation. *J. Geophys. Res. Atmos.,* **104,** 5131–5149, doi:10.1029/1998JC900090.

Wang, Y., L. Zhou, and K. Hamilton, 2007: Effect of convective entrainment/detrainment on simulation of tropical precipitation diurnal cycle. *Mon. Wea. Rev.,* **135,** 567–585, doi:10.1175/MWR3308.1.

——, C. N. Long, J. H. Mather, and X. Liu, 2011: Convective signals from surface measurements at ARM tropical western Pacific site: Manus. *Climate Dyn.,* **36,** 431–449, doi:10.1007/s00382-009-0736-z.

Wang, Z., and K. Sassen, 2001: Cloud type and macrophysical property retrieval using multiple remote sensors. *J. Appl. Meteor.,* **40,** 1665–1682, doi:10.1175/1520-0450(2001)040<1665:CTAMPR>2.0.CO;2.

Webb, M., and Coauthors, 2006: On the contribution of local feedback mechanisms to the range of climate sensitivity in two GCM ensembles. *Climate Dyn.,* **27,** 17–38, doi:10.1007/s00382-006-0111-2.

Wielicki, B. A., and Coauthors, 2002: Evidence for large decadal variability in the tropical mean radiative energy budget. *Science,* **295,** 841–844, doi:10.1126/science.1065837.

Zipser, E. J., C. Liu, D. J. Cecil, S. W. Nesbitt, and D. P. Yorty, 2006: Where are the most intense thunderstorms on Earth? *Bull. Amer. Meteor. Soc.,* **87,** 1057–1071, doi:10.1175/BAMS-87-8-1057.